J. Fluid Mech. (1986), *vol.* 162, *pp.* 35–51
Printed in Great Britain

Plane potential flows past doubly periodic arrays and their connection with effective transport properties

By F. K. LEHNER

Koninklijke/Shell Exploratie en Produktie Laboratorium,
2288 GD Rijswijk ZH, The Netherlands

(Received 20 May 1985)

A method of constructing plane potential flows past doubly periodic arrays of cylindrical obstacles is described. It is based on Rankine's well-known technique of determining by simple superposition the shape of an oval-shaped obstacle simultaneously with the flow round the obstacle. This paper deals with the use of such potentials in calculating effective medium conductivities for a class of doubly periodic two-phase materials which contain either non-conducting or perfectly conducting cylindrical inclusions embedded within a conducting matrix phase.

1. Introduction

Spatially periodic potential flows are encountered typically in inhomogeneous materials with periodic microstructure, when these conduct heat or electricity or, as in the case of certain porous materials, allow for matter transport by molecular diffusion through an interstitial fluid phase. Common to formally analogous transport phenomena of this kind is the problem of deriving an effective or bulk conductivity which enters as the factor of proportionality into the linear relation between the mean-field strength and the mean-flux density. The same type of problem arises with the determination of a number of distinct transport properties which characterize the linear theories of a variety of transport phenomena in two-phase materials. A unifying approach was discussed by Batchelor (1974) for the case of statistically homogeneous two-phase materials with random microstructure, aiming typically at close enough approximations or bounds for a particular property in terms of constituent phase properties and phase geometries. On the other hand, specific phase geometries and spatially periodic two-phase microstructures, in particular, will permit the exact determination of a transport property. These different categories of approach have recently been reviewed by McPhedran, McKenzie & Phaen-Thien (1983).

In the following, a method is described which yields exact effective conductivities for a class of two-phase materials with doubly periodic microstructure, corresponding to an arrangement on a lattice of identically shaped cylindrical inclusions of either infinite or zero conductivity, embedded in a conducting matrix phase. The method of construction by which this class may be characterized is identical with Rankine's well-known technique of determining the potential flow round oval-shaped bodies by superposition of the potential of a uniform flow and that of a suitable distribution of singularities. It appears that this technique, which has its origin in fluid dynamics, has not been used so far for the construction of potential flows round doubly periodic arrays of obstacles and that indeed the connection between such solutions and the effective-conductivity problem has never been explored.

'Rankine media', as one may label for convenience the class of two-phase materials constructed by a Rankine technique, are characterized by inclusion shapes which depend on volume fraction. This effect, which is due to interference among neighbouring inclusions, will be negligible at small volume fractions, but with increasing volume fractions manifests itself in an adjustment of the shape of an inclusion to that of the lattice cell. This feature clearly sets apart the two-phase media studied here from others which are characterized by fixed inclusion shapes and, beginning with Lord Rayleigh's (1892) pioneering work, have been much investigated.

The inclusion shapes found for Rankine media in the case of a rectangular lattice will, in general, display only a mirror symmetry with respect to the symmetry axes of a lattice cell and thus yield different effective conductivities in the x- and y-directions. The determination of the conductivity in the x-direction is carried out simultaneously with the construction of the inclusions in the present approach and accordingly will be dealt with first. A separate and general argument is introduced subsequently, which allows determination of the effective conductivity in the (transverse) y-direction from the value of the conductivity in the x-direction as well as from properties of the potential distribution associated with the latter. An extension of the underlying principle, with the goal of constructing three-dimensional Rankine media, seems well worth investigating, particularly perhaps in the context of applications of diffusion theory to biological porous materials with cellular microstructure (Nicholson & Phillips 1981).

2. Statement of the problem

Figure 1 shows a cross-section through a two-phase medium of the type to be discussed. The section is taken perpendicular to the axes of identical parallel cylinders, the outline C of which is symmetric in the x- and y- (lattice) axes. Only rectangular lattices, with lattice spacings $2a$ and $2b$ in the x- and y-directions, will be considered.

In general, let σ_1 and σ_2 denote the distinct conductivities of the two phases. The relevant potential $\Phi(x, y)$ then is an harmonic function, satisfying

$$\nabla^2 \Phi = 0, \tag{2.1}$$

in each region, and

$$\Phi_1 = \Phi_2, \quad \sigma_1 \frac{\partial \Phi}{\partial n} = \sigma_2 \frac{\partial \Phi}{\partial n} \quad \text{on } C, \tag{2.2), (2.3}$$

the derivatives being taken in the direction of a chosen unit vector normal to the smooth contour C.

Consider now the cases when a static field of spatially uniform average strength $\langle E_x \rangle$ or $\langle E_y \rangle$ is applied alternately parallel to the x- or y-direction. These averages may be defined for a single lattice cell Ω of surface area $4ab$. The segments of the boundary $\partial\Omega$ furnishing the entry and exit surfaces for the currents associated with these mean fields will be equipotential lines. For the lattice cell centred on the origin, one can therefore express the mean fields with the aid of Gauss's theorem as follows:

$$\begin{aligned} \langle E_x \rangle &= -\frac{1}{4ab} \int_\Omega \frac{\partial \Phi}{\partial x} \, \mathrm{d}A = -\frac{1}{4ab} \int_{\partial\Omega} \Phi n_x \, \mathrm{d}s \\ &= -\frac{1}{4ab} \left\{ \Phi(a) \int_{-b}^{b} \mathrm{d}y - \Phi(-a) \int_{-b}^{b} \mathrm{d}y \right\} = -\frac{\Delta_x \Phi}{2a}, \end{aligned} \tag{2.4}$$

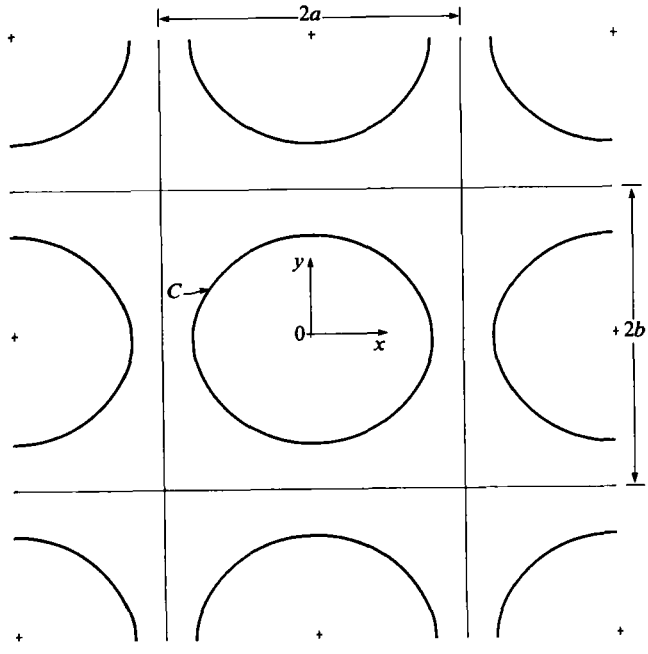

FIGURE 1. Rectangular array of oval-shaped inclusions embedded in a continuous matrix phase.

and, if the mean field is parallel to the y-direction,

$$\langle E_y \rangle = -\frac{1}{4ab}\int_\Omega \frac{\partial \Phi}{\partial y}\,\mathrm{d}A = -\frac{1}{4ab}\int_{\partial\Omega} \Phi n_y\,\mathrm{d}s$$

$$= -\frac{1}{4ab}\left\{-\Phi(-b)\int_{-a}^{a}\mathrm{d}x - \Phi(b)\int_{-a}^{a}\mathrm{d}x\right\} = -\frac{\Delta_y \Phi}{2b}. \tag{2.5}$$

Notice that the integrals extending over the matrix–inclusion interface C vanish because of condition (2.2).

The current density (J_x, J_y) in each phase can be expressed in terms of the function Ψ in accordance with the definition

$$J_x = -\sigma\frac{\partial \Phi}{\partial x} = -\frac{\partial \Psi}{\partial y}, \tag{2.6}$$

$$J_y = -\sigma\frac{\partial \Phi}{\partial y} = \frac{\partial \Psi}{\partial x}. \tag{2.7}$$

In the terminology of the hydrodynamic analogue, $\Psi(x, y)$ represents the harmonic conjugate 'stream function' associated with the 'velocity potential' $\sigma\Phi(x, y)$. Along the phase boundary therefore

$$\frac{\partial \Psi}{\partial s} = \sigma\frac{\partial \Phi}{\partial n},$$

where $\partial/\partial s$ denotes differentiation along C. It follows from (2.3) that

$$\Psi_1 = \Psi_2 \quad \text{on } C. \tag{2.8}$$

When the mean field is oriented in the x- or y-direction, the lattice-cell boundaries parallel to this field are local field lines $\Psi =$ constant and the corresponding mean current densities are therefore given by

$$\langle J_x \rangle = -\frac{1}{4ab}\int_\Omega \sigma \frac{\partial \Phi}{\partial x}\,\mathrm{d}A = -\frac{1}{4ab}\int_\Omega \frac{\partial \Psi}{\partial y}\,\mathrm{d}A = -\frac{1}{4ab}\int_{\partial\Omega} \Psi n_y\,\mathrm{d}s$$
$$= \frac{1}{4ab}\left\{\Psi(-b)\int_{-a}^{a}\mathrm{d}x - \Psi(b)\int_{-a}^{a}\mathrm{d}x\right\} = -\frac{\Delta_y \Psi}{2b} \tag{2.9}$$

and

$$\langle J_y \rangle = -\frac{1}{4ab}\int_\Omega \sigma \frac{\partial \Phi}{\partial y}\,\mathrm{d}A = \frac{1}{4ab}\int_\Omega \frac{\partial \Psi}{\partial x}\,\mathrm{d}A = \frac{1}{4ab}\int_{\partial\Omega} \Psi n_x\,\mathrm{d}s$$
$$= \frac{1}{4ab}\left\{\Psi(a)\int_{-b}^{b}\mathrm{d}y - \Psi(-a)\int_{-b}^{b}\mathrm{d}y\right\} = \frac{\Delta_x \Psi}{2a}, \tag{2.10}$$

where the integrals extending over C vanish again because of condition (2.8).

With the aid of (2.4), (2.5) and (2.9), (2.10), the effective conductivities in the x- and y-directions are now defined by

$$\sigma_x^*(\sigma_1, \sigma_2) = \frac{\langle J_x \rangle}{\langle E_x \rangle} = \frac{a}{b}\frac{\Delta_y \Psi}{\Delta_x \Phi} \tag{2.11}$$

and

$$\sigma_y^*(\sigma_1, \sigma_2) = \frac{\langle J_y \rangle}{\langle E_y \rangle} = -\frac{b}{a}\frac{\Delta_x \Psi}{\Delta_y \Phi}. \tag{2.12}$$

Since σ_x^* and σ_y^* have the dimensions of conductivities, they must be homogeneous functions of degree one in σ_1 and σ_2. Following Keller (1964), one may thus introduce standard conductivities defined by

$$\Sigma_x\left(1, \frac{\sigma_2}{\sigma_1}\right) = \frac{\sigma_x^*(\sigma_1, \sigma_2)}{\sigma_1}, \quad \Sigma_y\left(1, \frac{\sigma_2}{\sigma_1}\right) = \frac{\sigma_y^*(\sigma_1, \sigma_2)}{\sigma_1}. \tag{2.13}$$

The first argument of these functions may now be assumed to denote consistently the conductivity of the matrix phase and the second that of the inclusion phase. Σ_x and Σ_y may then be viewed as the conductivities of a medium with matrix conductivity equal to one and inclusion conductivities differing from one by a factor σ_2/σ_1.

An elegant result, due to Keller (1964) and later generalized by Mendelson (1975) relates the conductivity Σ_x of one medium to the conductivity Σ_y of another medium obtained from the first by exchanging the conductivities of the matrix and inclusion phases. Keller's theorem states that

$$\Sigma_x\left(1, \frac{\sigma_2}{\sigma_1}\right)\Sigma_y\left(1, \frac{\sigma_1}{\sigma_2}\right) = 1. \tag{2.14}$$

This study will focus on the determination of effective conductivities for media containing non-conducting inclusions. For this particular case Keller's theorem takes the form (Keller 1963)

$$\Sigma_x(1, 0)\,\Sigma_y(1, \infty) = 1, \tag{2.15}$$

and this useful reciprocal relation will permit the translation of all subsequent results for non-conducting inclusions into results for perfectly conducting inclusions.

In studying the effects of cylindrical obstacles Lord Rayleigh, and it would seem

essentially all later investigators, considered configurations as shown in figure 1, in either two or three dimensions, always assuming that the inclusion shape was given in advance. In the two-dimensional case, circular or elliptical cross-sections were naturally studied first. Even for these 'simple' shapes, considerable analytical efforts go into the calculation of effective conductivities and especially into the construction of estimates in the form of upper or lower bounds.

It is well known, on the other hand, and usually discussed for the formally analogous case of irrotational flow of an ideal fluid round oval-shaped bodies, that such a flow is determined most easily, if the body's shape is determined, as in a free-boundary problem, simultaneously with the flow through a construction introduced by Rankine. The classical example, found in most textbooks on fluid dynamics, is that of a plane flow round an oval 'Rankine body', obtained by superimposing the complex potentials of a uniform flow and of a source–sink pair. Thus, the shape of the oval is determined by a simple superposition and is allowed to vary with a certain parameter of the flow. Superposition of a uniform flow and a dipole at the origin, for example, yields the flow round a circular cylinder. The relevant complex potentials are $-Uz$ and $-M/2\pi z$ and yield the combined potential $\omega(z) = -M/2\pi z - Uz$. The streamline $\operatorname{Im}\omega(z) = -Uy\{1-(M/2\pi U)/(x^2+y^2)\} = 0$ runs along the x-axis and splits to define the circular contour of the resulting Rankine body. Its radius is equal to $(M/2\pi U)^{\frac{1}{2}}$ and is seen to depend on the relative strength of the dipole singularity to that of the uniform flow through the ratio of dipole moment M over speed or current density U.

Returning to figure 1 the idea to be explored in the following is now clear. It is to construct a two-phase material as an array of Rankine bodies by superposition of the complex potentials of a uniform flow and of a suitably selected doubly periodic array of isolated or distributed singularities. It follows, of course, that Rankine's method remains restricted to the construction of flows round non-conducting obstacles. The quantities of primary interest are thus the conductivities $\Sigma_x(1,0)$ and $\Sigma_y(1,0)$, or briefly Σ_x and Σ_y.

Since it suffices then to consider a matrix of conductivity $\sigma = 1$, the defining relations (2.11) and (2.12) may for the present purpose be written

$$\Sigma_x = \frac{a}{b}\frac{\Delta_y \Psi}{\Delta_x \Phi}, \tag{2.16}$$

$$\Sigma_y = -\frac{b}{a}\frac{\Delta_x \Psi}{\Delta_y \Phi}, \tag{2.17}$$

where the potential drops are due to a flow through a matrix of conductivity $\sigma = 1$. To cover all cases of $\sigma \neq 0$, one uses (2.13) to get

$$\sigma_x^*(\sigma,0) = \sigma\Sigma_x, \quad \sigma_y^*(\sigma,0) = \sigma\Sigma_y. \tag{2.18}$$

3. The conductivity of a medium containing cylindrical inclusions shaped as Rankine bodies

3.1. *An example*

Consider again the rectangular lattice with cell dimensions $2a \times 2b$, as shown in figure 1, and assume now that there are logarithmic sources of strength $-Q$ located at $z = -\frac{1}{2}c$ and all equivalent points and sinks of strength Q at $z = +\frac{1}{2}c$ and all equivalent points throughout the complex z-plane, where $z = x + iy$ and c is a real

constant satisfying $0 < c < 2a$. The complex potential $\omega_0 = \Phi_0 + \mathrm{i}\Psi_0$ of this doubly periodic distribution of singularities is given by

$$\omega_0(z) = \frac{Q}{2\pi} \ln \frac{\vartheta_1[(z+\frac{1}{2}c)/2a]}{\vartheta_1[(z-\frac{1}{2}c)/2a]}, \tag{3.1}$$

where $\vartheta_1(v,\tau)$ is a Jacobian Theta function of the reduced argument v and parameter τ, as defined by

$$v = \frac{z}{2a}, \quad \tau = \frac{\mathrm{i}b}{a}, \tag{3.2), (3.3}$$

the dependence on τ being suppressed by the customary notation $\vartheta_1(v)$. The function $\vartheta_1(v)$ is an entire transcendental function with the properties (Abramowitz & Stegun 1970)

$$\vartheta_1(-v) = -\vartheta_1(v), \tag{3.4}$$

$$\vartheta_1(v+1) = -\vartheta_1(v), \tag{3.5}$$

$$\vartheta_1(v+\tau) = -q^{-1}\,\mathrm{e}^{-2\mathrm{i}\pi v}\,\vartheta_1(v), \tag{3.6}$$

where the nome q is defined by

$$q = \mathrm{e}^{\pi b/a}. \tag{3.7}$$

Thus, $\vartheta_1(v)$ is odd and periodic in v with the real period 2. These properties imply the following important behaviour of the complex potential ω_0 within the basic lattice cell, as may readily be shown:

$$\Phi_0(0,y) = 0, \tag{3.8}$$

$$\Psi_0(x,0) = 0, \tag{3.9}$$

$$\Delta_x \Phi_0 \equiv \Phi_0(a) - \Phi_0(-a) = 0 - 0 = 0, \tag{3.10}$$

$$\Delta_y \Psi_0 \equiv \Psi_0(b) - \Psi_0(-b) = \frac{Qc}{2a}. \tag{3.11}$$

According to (3.11) a net flux of magnitude $Qc/2a$ passes through the cell in the negative x-direction. One can cancel this flux by superposition of a constant field of strength $Qc/4ab$ oriented in the positive x-direction. Addition of the complex potential $-(Qz/4ab)\,z$ of this field to ω_0 then furnishes a potential

$$\omega_1(z) = -Q\left\{\frac{1}{2\pi} \ln \frac{\vartheta_1[(z+\frac{1}{2}c)/2a]}{\vartheta_1[(z-\frac{1}{2}c)/2a]} + \frac{cz}{4ab}\right\}, \tag{3.12}$$

with the property

$$\Delta_y \Psi_1 \equiv \Psi_1(b) - \Psi_1(-b) = 0. \tag{3.13}$$

Consider now the potential

$$\omega(z) = \Phi(x,y) + \mathrm{i}\Psi(x,y) = \omega_1(z) - Uz, \tag{3.14}$$

where $U \geqslant 0$ is some constant current density. For this new potential

$$\Delta_x \Phi \equiv \Phi(a) - \Phi(-a) = -\left(1 + \frac{Qc}{4abU}\right) 2aU, \tag{3.15}$$

and

$$\Delta_y \Psi \equiv \Psi(b) - \Psi(-b) = -2bU. \tag{3.16}$$

The field associated with ω is thus seen to drive a current of density U in the positive x-direction, while the potential difference across the cell is given by (3.15). According to definition (2.16), the lattice cell therefore has the effective conductivity

$$\Sigma_x = \left(1 + \frac{Qc}{4abU}\right)^{-1} \tag{3.17}$$

and, by virtue of (2.4), (3.15) may thus be cast precisely in the form of the appropriate macroscopic law:

$$U = \Sigma_x \langle E_x \rangle. \tag{3.18}$$

The key property of the potential (3.14) is that it permits the field $\langle E_x \rangle$ and the current density U to be varied proportionally, in accordance with (3.18), while Σ_x is held fixed by adjusting the independent parameter Q in such a way as to maintain a constant ratio Q/U. The potential ω therefore serves to construct an obstructed flow of average current density U through a medium with effective conductivity $\Sigma_x < 1$. In the unobstructed case $\omega_1 = 0$ or $\omega = -Uz$ and $\Sigma_x = 1$ accordingly. Thus $\omega_1(z)$ plays a role in the construction of the two-phase medium analogous to that of the dipole potential $-M/2\pi z$ in Rankine's construction of the flow round a single cylindrical obstacle.

3.2. *Inclusion shapes parametrized by* Σ_x

In determining the inclusion shape and effective conductivity for a given potential, it proves convenient to rescale the lattice by defining

$$v = \frac{z}{2a} = x + \mathrm{i}y, \tag{3.19}$$

$$d = \frac{c}{2a}, \tag{3.20}$$

where x and y now have the ranges

$$-\tfrac{1}{2} \leqslant x \leqslant \tfrac{1}{2}, \quad -\frac{b}{2a} \leqslant y \leqslant \frac{b}{2a}$$

for the basic cell. Accordingly, upon substitution for ω_1 from (3.12), the potential (3.14) is written

$$\omega = \Phi(x,y) + \mathrm{i}\Psi(x,y) = -Q\left[\frac{1}{2\pi} \ln \frac{\vartheta_1(v+\frac{1}{2}d)}{\vartheta_1(v-\frac{1}{2}d)} + \frac{adv}{b}\right] - 2aUv. \tag{3.21}$$

The complete doubly periodic array of identical inclusions associated with this potential is determined by the streamlines

$$\Psi_{(n)} = \operatorname{Im}\omega = -n2bU \quad (n = 0, \pm 1, \pm 2, \ldots), \tag{3.22}$$

but it suffices to focus on the inclusion centred on the origin within the basic lattice cell. Its shape is seen to be determined by the condition $\operatorname{Im}\omega = 0$, or

$$y + \frac{Q/2aU}{1 + Qd/2bU} \frac{1}{2\pi} \operatorname{Im} \ln \frac{\vartheta_1(v+\frac{1}{2}d)}{\vartheta_1(v-\frac{1}{2}d)} = 0,$$

which, with the aid of definitions (3.17) and (3.20), can be brought into the form

$$\Sigma_x = 1 + y \Big/ \left[\frac{b}{2\pi ad} \operatorname{Im} \ln \frac{\vartheta_1(v+\frac{1}{2}d)}{\vartheta_1(v-\frac{1}{2}d)}\right]. \tag{3.23}$$

This transcendental equation for the inclusion contour contains as parameters the aspect ratio b/a, the distance d between source and sink, and the effective conductivity Σ_x. Thus, at fixed values of b/a and d, the size and shape of the inclusion is uniquely determined by the value of Σ_x.

Numerical solutions to (3.23) are readily obtained upon extraction of the imaginary part of the rapidly converging Fourier series (Abramowitz & Stegun 1970)

$$\ln\frac{\vartheta_1(v+\frac{1}{2}d)}{\vartheta_1(v-\frac{1}{2}d)} = \ln\frac{\sin\pi(v+\frac{1}{2}d)}{\sin\pi(v-\frac{1}{2}d)} + 4\sum_{n=1}^{\infty}\frac{1}{n}\frac{q^{2n}}{1-q^{2n}}\sin 2n\pi v\sin n\pi d, \tag{3.24}$$

where q is defined by (3.7).

The special case of a doubly periodic array of dipoles situated in the cell centres may be recovered from the above results by passing to the limit $d\to 0$, while requiring

$$\lim_{d\to 0}(2Qad) = M = \text{constant}.$$

In this limit, (3.21) becomes

$$\omega = \Phi(x,y)+\mathrm{i}\Psi(x,y) = -\frac{M}{2a}\left[\frac{1}{2\pi}\frac{\vartheta_1'(v)}{\vartheta_1(v)}+\frac{av}{b}\right]-2aUv. \tag{3.25}$$

In the same limit one obtains from (3.23) the following relation for the inclusion shape and associated conductivity:

$$\Sigma_x = 1+y\Big/\left[\frac{b}{2\pi a}\operatorname{Im}\frac{\vartheta_1'(v)}{\vartheta_1(v)}\right]. \tag{3.26}$$

The logarithmic derivative of the Theta function has the Fourier series representation (Abramowitz & Stegun 1970)

$$\frac{\vartheta_1'(v)}{\vartheta_1(v)} = \pi\cot\pi v + 4\pi\sum_{n=1}^{\infty}\frac{q^{2n}}{1-q^{2n}}\sin 2n\pi v. \tag{3.27}$$

A solution to (3.26)–(3.27) for a square lattice with $b/a = 1$, and for the value $\Sigma_x = 0.43$ is shown in figure 2. Also shown are a number of equipotential lines, $\Phi(x,y)/2aU = \text{constant}$, and streamlines, $\Psi(x,y)/2aU = \text{constant}$. The equipotential lines could clearly serve as field lines or streamlines in a transverse flow with perfectly conducting inclusions. Thus, the picture shown in figure 2 provides a visual demonstration of the content of Keller's theorem (2.15). As may be seen, (3.26) yields indeed an oval-shaped 'Rankine body'.

Figure 3 shows a sequence of inclusion shapes for different values of Σ_x and inclusion volume fractions f, the latter being readily obtained from (3.26) by numerical quadrature. Characteristically, the inclusions remain circular until occupying about 20% of the surface area of the cell; beyond this value there is noticeable flattening. Moreover, there exists a value of Σ_x at which the inclusions of neighbouring cells touch at the intersections of their horizontal axes with the cell boundaries, i.e. in the points $(-\frac{1}{2},0)$ and $(\frac{1}{2},0)$ and all equivalent points. This value of Σ_x therefore determines a threshold at which the conductivity Σ_y in the transverse direction vanishes. It also marks the lower limit of validity of (3.23) and (3.26). Still lower values of Σ_x would be determined from slightly modified relations but the corresponding inclusions form continuous barriers in the x-direction and are of little immediate interest. Attention will therefore be given only to inclusion shapes corresponding to values of Σ_x larger than or equal to the threshold value.

The points of intersection of the inclusion contour C with the x-axis, i.e. the stagnation points $(x_s,0)$, enter into an expression for the conductivity

$$\Sigma_x = 1-\frac{ad}{b}\Big/\left[\frac{\sin\frac{1}{2}\pi d\cos\frac{1}{2}\pi d}{\sin^2\pi x_s-\sin^2\frac{1}{2}\pi d}-4\sum_{n=1}^{\infty}\frac{q^{2n}}{1-q^{2n}}\cos 2n\pi x_s\sin n\pi d\right], \tag{3.28}$$

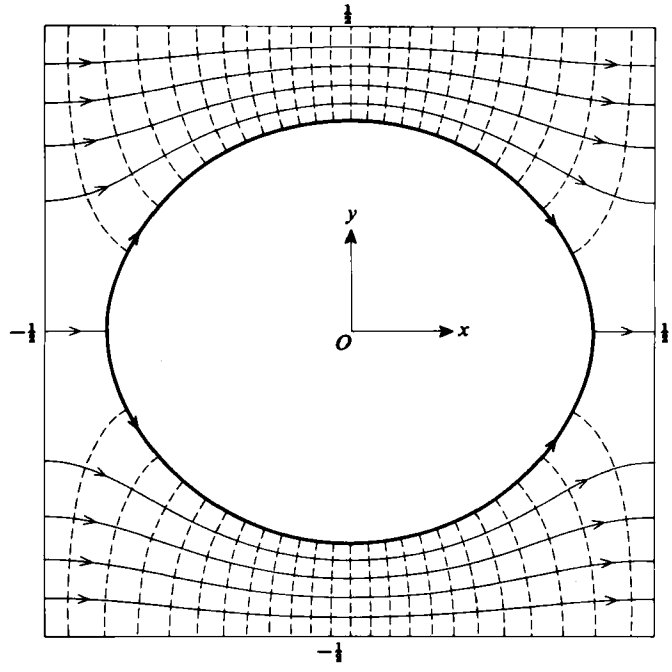

FIGURE 2. Plane potential flow round an inclusion in a lattice cell, constructed by superposition of a doubly periodic dipole flow ($d = 0$) and a parallel flow in the x-direction. Conductivities $\Sigma_x = 0.43$, $\Sigma_y = 0.34$ and inclusion volume fraction $f = 0.43$.

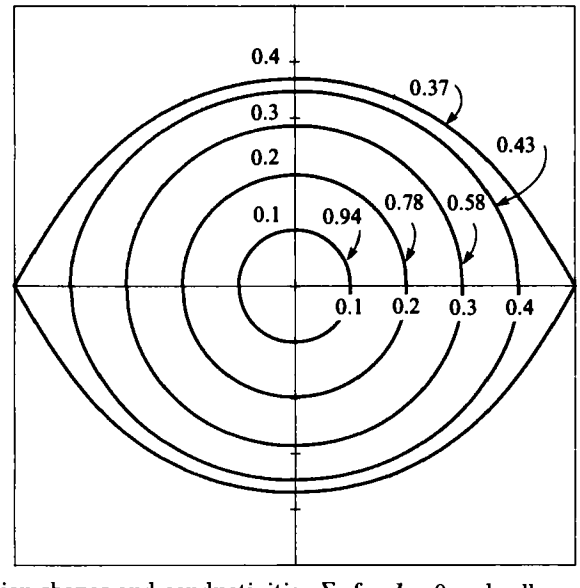

FIGURE 3. Inclusion shapes and conductivities Σ_x for $d = 0$ and cell aspect ratio $b/a = 1$.

which may be derived from (3.23) upon taking the limit $y \to 0$. From this follows the threshold value of Σ_x for $x_s = \pm\frac{1}{2}$:

$$\Sigma_x(\text{threshold}) = 1 - \frac{ad}{b} \Big/ \left[\tan \tfrac{1}{2}\pi d - 4 \sum_{n=1}^{\infty} (-1)^n \frac{q^{2n}}{1-q^{2n}} \sin n\pi d \right]. \tag{3.29}$$

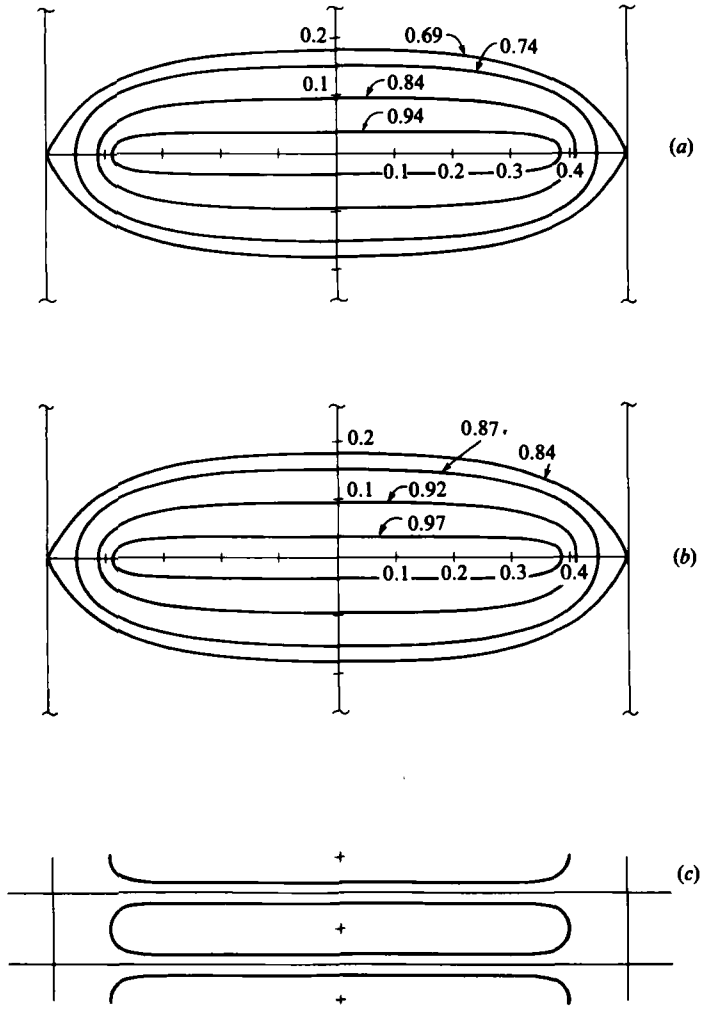

FIGURE 4. Effect of cell aspect ratio on inclusion shapes and conductivities Σ_x for $d = 0.75$. (a) $b/a = 1$; (b) $b/a = 2$; (c) $b/a = 0.125$, $\Sigma_x = 0.35$.

The corresponding results for the dipole array are

$$\Sigma_x = 1 - \frac{2a}{\pi b} \Big/ \left[\frac{1}{\sin^2 \pi x_s} - 8 \sum_{n=1}^{\infty} \frac{q^{2n}}{1-q^{2n}} \cos 2n\pi x_s \right], \tag{3.30}$$

and

$$\Sigma_x(\text{threshold}) = 1 - \frac{2a}{\pi b} \Big/ \left[1 - 8 \sum_{n=1}^{\infty} (-1)^n \frac{q^{2n}}{1-q^{2n}} \right]. \tag{3.31}$$

Figure 4 provides an illustration of the type of oval-shaped inclusion generated by the potential (3.21) of a source–sink pair with separation $d = 0.75$. It also illustrates the effect of the aspect ratio b/a of the lattice on inclusion shape and conductivity. On comparing figure 4 (*a*) with figure 4 (*b*), only small differences in shape are detected at the maximum inclusion size. Notice that comparable inclusions are constructed with equal width in the x-direction. The difference between the configurations shown in figures 4 (*a*) and 4 (*b*) therefore essentially amounts to an increase in lattice spacing

or anisotropic dilution, the effect of which is clearly reflected in the conductivities for comparable inclusion shapes.

A shortening of the lattice spacing in the y-direction, on the other hand, changes inclusion shapes significantly at aspect ratios $b/a < 1$, as may be seen from figure 4(*c*) which depicts the slender inclusion shape obtained for the particular value $\Sigma_x = 0.34$ at $f = 0.55$.

3.3. *Determination of* Σ_y

According to the definition already given

$$\Sigma_y = -\frac{b}{a}\frac{\Delta_x \Psi}{\Delta_y \Phi}, \tag{2.17}$$

where $\Delta_y \Phi \equiv \Phi(b) - \Phi(-b)$ and $\Delta_x \Psi \equiv \Psi(a) - \Psi(-a)$ are the changes in the potential and its harmonic conjugate across the lattice cell and the y- and x-direction, respectively, which occur for a uniform field, $\langle E_y \rangle$, oriented in the y-direction.

The idea is now to determine the ratio $\Delta_x \Psi / \Delta_y \Phi$ by mapping the region of flow conformally onto a rectangle in such a way that the mapped field becomes a constant field. Given that the field is parallel to two sides of this as yet undetermined rectangular region of aspect ratio K'/K, say, one has

$$\Delta_x \Psi / \Delta_y \Phi = -K/K', \tag{3.32}$$

from (2.17) and by virtue of the fact that $\Sigma_y = 1$ for an unobstructed flow. Therefore

$$\Sigma_y = \frac{b}{a}\frac{K}{K'}, \tag{3.33}$$

Relation (3.32) is, of course, based on the fact that the boundary values of Φ and Ψ remain unchanged under conformal mappings.

The required mapping will be a composite mapping, beginning with the potential $\omega(z)$. Thus, consider the function

$$\zeta(z) = \frac{\omega}{2aU} + \frac{1}{2\Sigma_x}, \tag{3.34}$$

which maps the cell $\{0 \leqslant x \leqslant 2a,\ -b \leqslant y \leqslant b\}$ contained in figure 1 onto the rectangle $\{-1/2\Sigma_x \leqslant \operatorname{Re}\zeta \leqslant 1/2\Sigma_x,\ -b/2a \leqslant \operatorname{Im}\zeta \leqslant b/2a\}$ shown in figure 5(*a*). The images of the field lines of the actual flow in the y-direction now pass through a central constriction of width $2r$ created by plane barriers, each of which represents the image of one half of an inclusion. The length of these barriers is known from the fact that the point $\zeta = r$ is the image of the stagnation point $(x_s, 0)$ which lies at the intersection of the central inclusion contour C with the positive x-axis (cf. figure 2). Accordingly,

$$r = \frac{\Phi_s}{2aU} + \frac{1}{2\Sigma_x}, \tag{3.35}$$

where $\Phi_s = \Phi(x_s, 0)$ is the potential in the stagnation point. From (3.21) and (3.24)

$$\frac{\Phi_s}{2aU} = -\frac{b}{2\pi ad}\left[\ln\frac{\sin\pi(x_s + \tfrac{1}{2}d)}{\sin\pi(x_s - \tfrac{1}{2}d)} + 4\sum_{n=1}^{\infty}\frac{1}{n}\frac{q^{2n}}{1-q^{2n}}\sin 2n\pi x_s \sin n\pi d\right]\left(\frac{1}{\Sigma_x} - 1\right) - \frac{x_s}{\Sigma_x}, \tag{3.36}$$

where Σ_x is given by (3.28), so that Φ_s and hence r is essentially determined from (3.28) and (3.36), starting from a given value of either x_s or Σ_x.

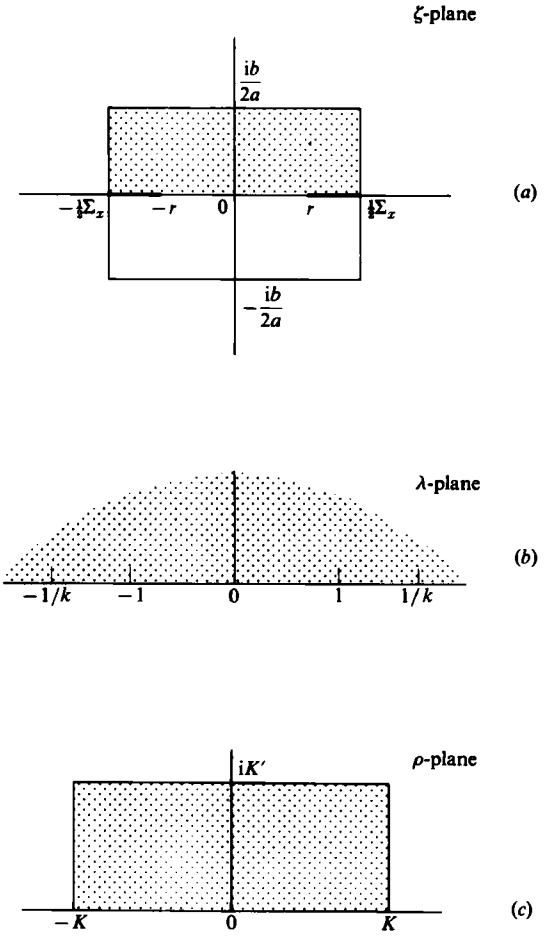

FIGURE 5.

In the next step, the upper half of the rectangle in figure 5(*a*) is mapped onto a half-plane $\operatorname{Im}\lambda \geqslant 0$ by means of the function

$$\lambda(\zeta) = \frac{\operatorname{sn}(2\Sigma_x \bar{K}\zeta, \bar{k})}{\operatorname{sn}(2\Sigma_x \bar{K}r, \bar{k})}, \tag{3.37}$$

where $\operatorname{sn} u = \operatorname{sn}(u, \bar{k})$ is a Jacobian elliptic function of modulus $\bar{k}$, the latter being determined by the transcendental equation

$$\frac{\bar{K}}{\bar{K}'} = \frac{a}{\Sigma_x b}, \tag{3.38}$$

where $\bar{K} = K(\bar{k})$ is the complete elliptic integral of the first kind of modulus $\bar{k}$ and $\bar{K}' = K'(\bar{k}) = K(\bar{k}')$, $\bar{k}' = \sqrt{(1-\bar{k}^2)}$ denoting the complementary modulus. The mapping (3.37) carries the points $0, \pm r, \pm 1/2\Sigma_x, \pm 1/2\Sigma_x + ib/2a$ into the points $0, \pm 1, \pm 1/k, \pm\infty$ on the real axis $\operatorname{Im}\lambda = 0$, as shown in figure 5(*b*). Here

$$k = \bar{k}\operatorname{sn}(2\Sigma_x \bar{K}r, \bar{k}). \tag{3.39}$$

The half-plane $\operatorname{Im}\lambda \geqslant 0$ may now be mapped again onto a rectangle by means of the Schwarz–Cristoffel mapping

$$\rho = F(\lambda, k) = \int_0^{\lambda} \frac{\mathrm{d}t}{[(1-t^2)(1-k^2t^2)]^{\frac{1}{2}}}, \tag{3.40}$$

which is seen to represent an elliptic integral of the first kind of modulus k. In particular, $K(k) = F(1, k)$ and $K'(k) = F(1, k')$ are complete elliptic integrals of modulus k and k', respectively. The choice (3.39) of modulus k ensures that the images under (3.40) of the points ± 1 and $\pm 1/k$ on $\operatorname{Im}\lambda = 0$ forms the corners $\pm K$, $\pm K + \mathrm{i}K'$ of a rectangle, shown in figure 5(*c*). In this rectangle the image of the original field in the z-plane appears as a uniform field with field lines parallel to $\operatorname{Re}\rho = 0$. Thus, the unknown rectangle of (3.32) has been determined.

Σ_y is now obtained for a given value of either x_s or Σ_x by first calculating $\Phi_s/2aU$ from (3.28) and (3.36) as well as r from (3.35). Next, one determines $\bar{k}$ and k from (3.38) and (3.39), using tables or appropriate series (Abramowitz & Stegun 1970). Then $K'/K(k)$ may be computed from (Oberhettinger & Magnus 1949),

$$\exp\left\{-\frac{\pi K'}{K}\right\} = \tfrac{1}{2}L + \frac{2}{2^5}L^5 + \frac{15}{2^9}L^9 + \frac{150}{2^{13}}L^{13} + \frac{1707}{2^{17}}L^{17} + \ldots, \tag{3.41}$$

with $L = [1-(1-k^2)^{\frac{1}{4}}]/[1+(1-k^2)^{\frac{1}{4}}]$, and finally Σ_y is obtained from (3.33).

It will be clear, of course, that the mapping technique used for determining Σ_y from known properties of a field in the x-direction remains applicable to a much larger class of inclusion shapes than considered here, subject only to the necessary symmetry in the x- and y-axes. Essentially, one requires Σ_x together with the potential $\Phi_s/2aU$ in the stagnation point $(x_s, 0)$ by any method. Consider, for example, the special case of a medium containing flat inclusions in the form of barriers of negligible thickness and dimensionless width d in the x-direction. There being no obstruction in the x-direction, Σ_x must equal unity while $\Phi_s/2aU = -\frac{1}{2}d$ at the stagnation point $x_s = \frac{1}{2}d$, i.e. along one edge of the central inclusion. In this case, therefore, Σ_x and $\Phi_s/2aU$ are trivially known and Σ_y may be computed immediately by the above method, using the values $\Sigma_x = 1$ and $r = \frac{1}{2}(1-d)$.

Finally, the asymptotic behaviour of $\Sigma_x(1, \infty)$ or $\Sigma_y(1, 0)$ for nearly touching inclusions is of some interest, being determined largely by the resistance of narrow-gap regions between adjoining inclusions. Let $h = 1-2|x_s|$ denote the gap width along the x-axis between two inclusions. Since $\Sigma_x(1, \infty) = 1/\Sigma_y(1, 0) \to \infty$ for $h \to 0$, it follows from (3.33) that $K'/K \to \infty$ or $k \to 0$, as implied by the asymptotic relation

$$\frac{K'}{K} = \frac{2}{\pi}\ln\frac{4}{k} + \ldots, \quad k \ll 1, \tag{3.42}$$

which is contained in (3.41). Furthermore, from (3.36), one has approximately $\Phi_s/2aU = -x_s/\Sigma_x$, assuming that $h \ll 1-d < 1$. Equations (3.35) and (3.39) therefore yield the approximation $k = \bar{k}\bar{K}h$, $h \ll 1$, where the modulus $\bar{k}$ and associated complete elliptic integral $\bar{K}$ are determined from (3.38) for the threshold value (3.29) of Σ_x. Introducing this approximation into (3.42) and substituting in (3.33), one obtains

$$\Sigma_x(1, \infty) = \frac{1}{\Sigma_y(1, 0)} = -\frac{2a}{\pi b}\ln h + \ldots, \quad h \ll 1, \tag{3.43}$$

upon neglecting a term which remains finite as h approaches zero.

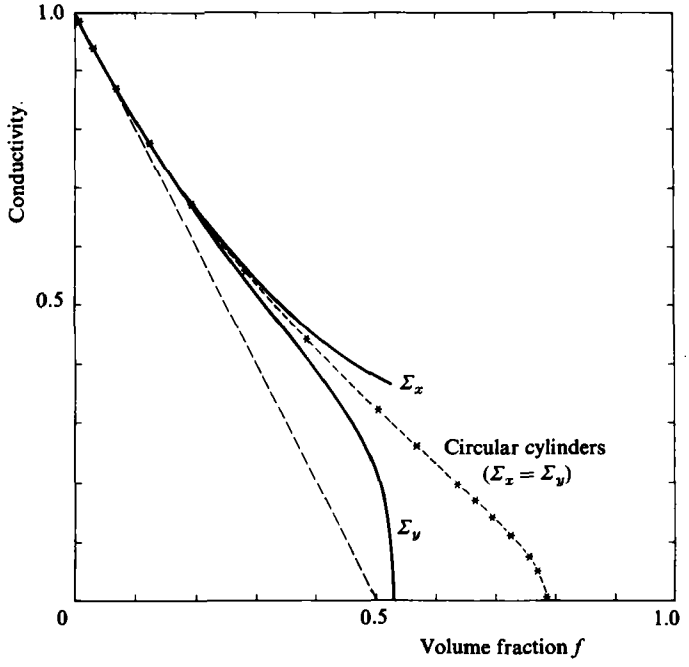

FIGURE 6. Conductivities Σ_x and Σ_y as functions of inclusion volume fraction f for a square array of Rankine bodies; $b/a = 1$, $d = 0$. Shown for comparison are the results of Keller & Sachs (1964) for circular cylinders.

The singularity exhibited by this result in the limit $h \to 0$ is expected for perfectly conducting inclusions and is well known since Keller (1963) first gave asymptotic results of this type for nearly touching, perfectly conducting spheres as well as circular cylinders. Keller's work was later extended considerably by Batchelor & O'Brien (1977), who obtained approximate results for nearly touching as well as for touching grains of large but finite conductivity in comparison with that of an embedding matrix phase (see also the recent discussion by McPhedran *et al.* 1983). The logarithmic singularity of (3.43) differs from the $h^{-\frac{1}{2}}$ singularity obtained by Keller for nearly touching circular cylinders but, coincidentally, is of the same form as in the case of a simple cubic array of nearly touching spheres, although its intensity is smaller by a factor $4/\pi^2$ and also involves a finite aspect ratio of the cell, the limit $a/b \to 0$ being disregarded here as of no particular significance.

It is seen that relation (3.43) does not depend upon d under the assumption that $h \ll 1-d$. The asymptotic behaviour of $\Sigma_x(1, \infty)$ may, in fact, be viewed as controlled by the gap width left between protuberances which grow from two adjoining inclusions and became pointed as $h \to 0$ while there is negligible change in inclusion volume fraction, as will become evident from the subsequent discussion. As with earlier results of this kind, it is the explicit prediction of the dependence of an effective medium property upon a type of constriction or 'pore throat', which makes relation (3.43) of some interest.

3.4. *Results for Σ_x and Σ_y*

It is instructive to consider first the case $d = 0, b/a = 1$ of figure 3. Here the inclusions are very nearly circular in cross-section at volume fractions less than 0.2. Hence, since the lattice is a square lattice, one expects approximately equal values of Σ_x and Σ_y

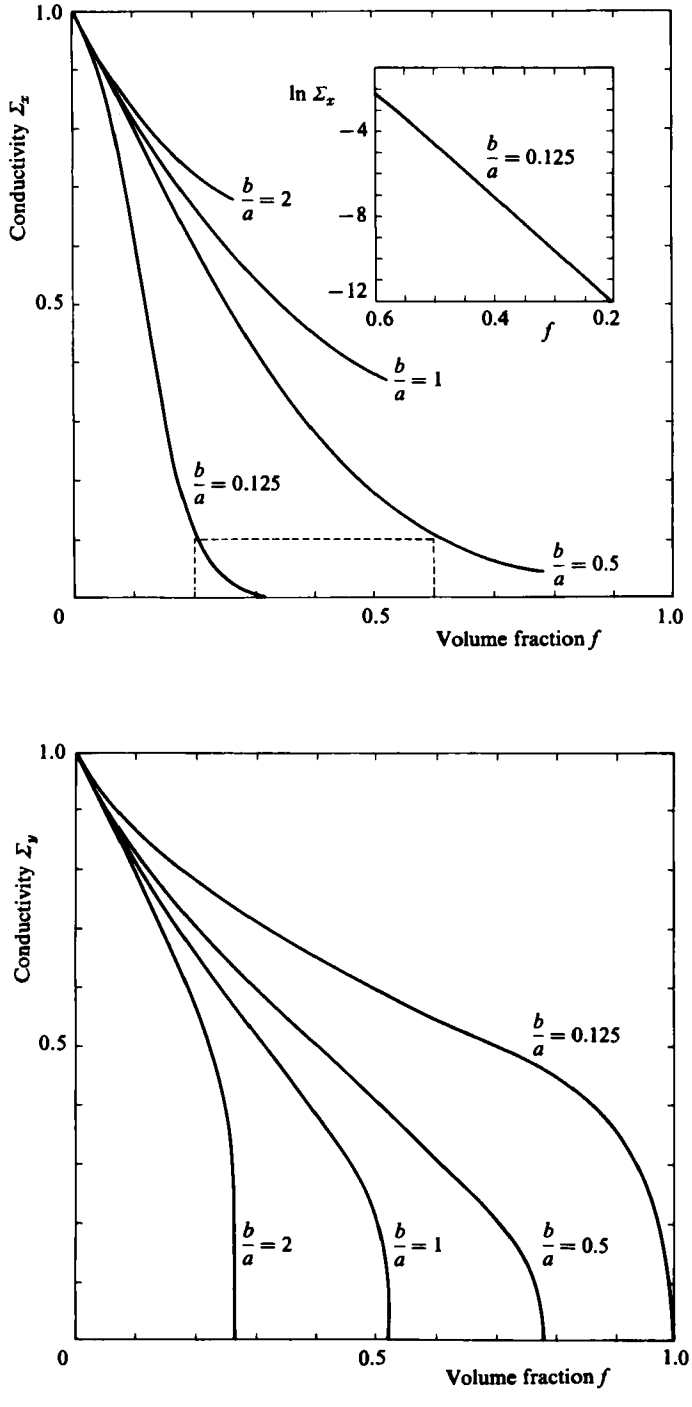

FIGURE 7. Conductivities Σ_x and Σ_y as functions of inclusion volume fraction f for various aspect ratios b/a and $d = 0$.

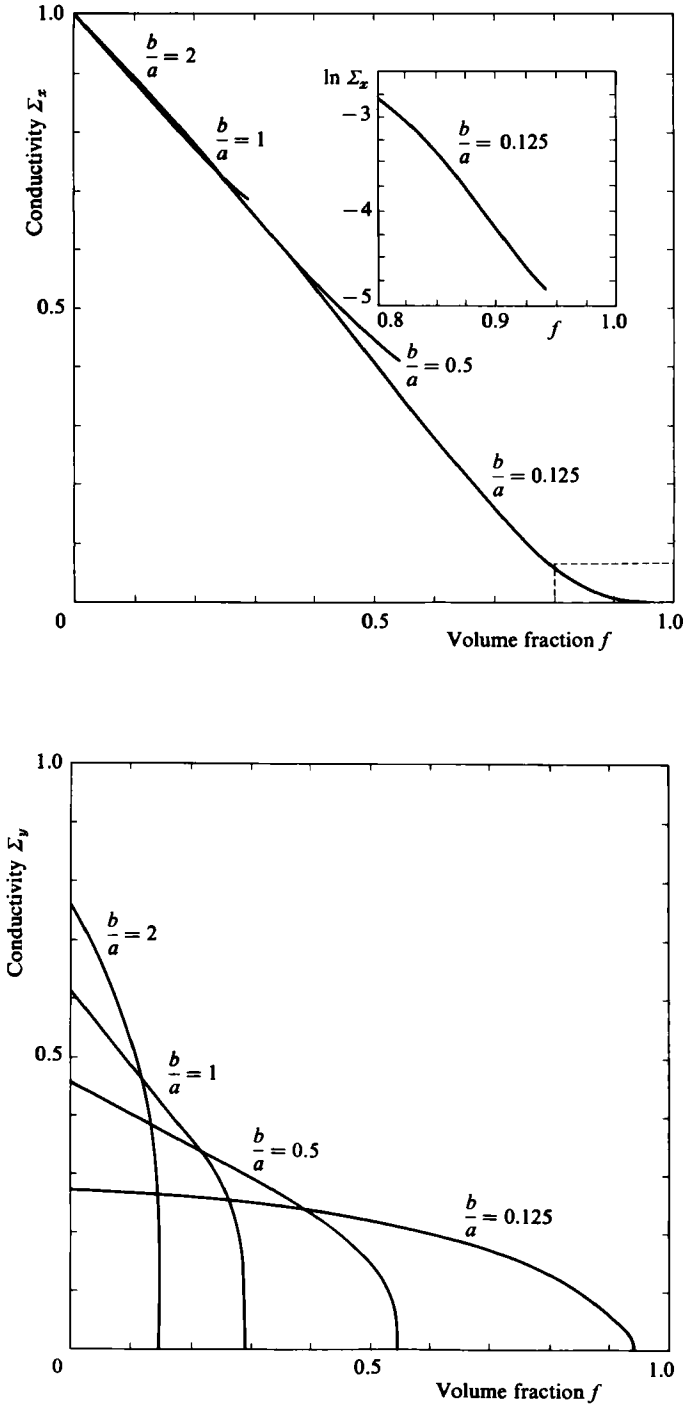

FIGURE 8. Conductivities Σ_x and Σ_y as functions of inclusion volume fraction f for various aspect ratios b/a and $d = 0.75$.

throughout this range. Figure 6 shows that this is indeed the case. Moreover, there is full agreement in this range with existing solutions for circular inclusions as may be seen from a comparison with data reported by Keller & Sachs (1964). The slope of all three curves approaches the value -2 as $f \to 0$, indicated by the straight dashed line, as may be readily inferred from expression (3.30) by considering values of x_s small enough to permit the approximations $\Sigma_x \approx 1 - 2\pi x_s^2 a/b \approx 1 - 2f$.

Figures 7 and 8 explore the effects of cell shape b/a and inclusion shape d on Σ_x and Σ_y. The different behaviour of Σ_x and Σ_y reflects the already familiar inclusion shapes and their evolution from horizontal barriers of width d and negligible thickness at $\Sigma_x \to 1$ to blocking barriers at the threshold $\Sigma_y = 0$. Thus, as the volume fraction approaches zero, Σ_y approaches a limit $\Sigma_y(f = 0) < 1$ whenever $d > 0$, corresponding to the existence of a barrier in the form of a sheet of negligible thickness, connecting the source and the sink.

Cell shapes with smaller aspect ratios b/a permit higher threshold volume fractions to be attained and conductivities below 0.1 display an exponential dependence on the volume fraction.

Furthermore, as may be seen from figure 8, apart from large differences in threshold conductivities, the effects of cell shape on Σ_x are much less pronounced for long and flat inclusions ($d = 0.75$), leading to a roughly linear dependence of Σ_x on f, independent of cell shape. In contrast herewith, figure 8 shows strikingly different behaviour of Σ_y depending on cell shape.

Dr J. M. Mosquera computed the numerical results from which the figures were drawn. His generous assistance is gratefully acknowledged. This work was supported by an unrestricted grant from Shell Development Company during the author's affiliation with the Division of Engineering at Brown University.

REFERENCES

ABRAMOWITZ, M. & STEGUN, I. A. 1970 *Handbook of Mathematical Functions*. Dover Publications.

BATCHELOR, G. K. 1974 Transport properties of two-phase materials with random structure. *Ann. Rev. Fluid Mech.* **6**, 227.

BATCHELOR, G. K. & O'BRIEN, R. W. 1977 Thermal or electrical conduction through a granular material. *Proc. R. Soc. Lond.* A **355**, 313.

KELLER, J. B. 1963 Conductivity of a medium containing a dense array of perfectly conducting spheres or cylinders or nonconducting cylinders. *J. Appl. Phys.* **34**, 991.

KELLER, J. B. 1964 A theorem on the conductivity of a composite medium. *J. Math. Phys.* **5**, 548.

KELLER, H. B. & SACHS, D. 1964 Calculations of the conductivity of a medium containing cylindrical inclusions. *J. Appl. Phys.* **35**, 537.

MCPHEDRAN, R. C., MCKENZIE, D. R. & PHAN-THIEN, N. 1983 Transport properties of two-phase composite materials. In *Advances in the Mechanics and the Flow of Granular Materials* ed. M. Shahinpoor, vol. 1, pp. 415. Gulf Publishing Co.

MENDELSON, K. S. 1975 Effective conductivity of a two-phase material with cylindrical phase boundaries. *J. Appl. Phys.* **46**, 917.

NICHOLSON, C. & PHILLIPS, J. M. 1981 Ion diffusion modified by tortuosity and volume fraction in the extracellular microenvironment of the rat cerebellum. *J. Physiol.* (London), **321**, 225.

OBENHETTINGER, F. & MAGNUS, W. 1949 *Anwendung der Elliptischen Funktionen in Physik und Technik*. Springer-Verlag.

RAYLEIGH, LORD 1982 On the influence of obstacles arranged in rectangular order on the properties of the medium. *Phil. Mag.* **34**, 481.